Korean J. Chem. Eng., 32(2), 261-267 (2015)
DOI: 10.1007/s11814-014-0220-2

pISSN: 0256-1115
eISSN: 1975-7220

Molecular structure-device performance relationship in polymer solar cells based on indene-C_{60} bis-adduct derivatives

Han-Hee Cho*, Chul-Hee Cho*, Hyunbum Kang*, Hojeong Yu, Joon Hak Oh**, and Bumjoon J. Kim*,†**

*Department of Chemical and Biomolecular Engineering, Korea Advanced Institute of Science and Technology (KAIST), Daejeon 305-701, Korea
**Department of Chemical Engineering, Pohang University of Science and Technology (POSTECH), Pohang, Gyeongbuk 790-784, Korea
(*Received 26 May 2014 • accepted 30 July 2014*)

Abstract−Interfacial tension between two materials is a key parameter in determining their miscibility and, thus, their morphological behavior in blend films. In bulk heterojunction (BHJ)-type polymer solar cells (PSCs), control of the interfacial tension between the electron donor and the electron acceptor is critically important in order to increase miscibility and achieve optimized BHJ morphology for producing efficient exciton dissociation and charge transport. Herein, we report the synthesis of a series of indene-C_{60} bis-adducts (ICBA) derivatives by modifying their end-groups with fluorine (FICBA), methoxy (MICBA) and bromine (BICBA) functional units. We systematically studied the effects of their structural changes on the blend morphology with poly(3-hexylthiophene) (P3HT) and their performance in the PSCs. The end-group modification of ICBA derivatives induced a dramatic change in their interfacial tensions with P3HT (i.e., from 4.9 to 8.3 mN m^{-1}), resulting in large variations in the power conversion efficiency (PCE) of the PSCs, ranging from 2.9 to 5.2%.

Keywords: Electron Acceptors, End Group Modification, Fullerene Bis-adducts, Interfacial Tension, Polymer Solar Cell

INTRODUCTION

Polymer solar cells (PSCs) have attracted considerable attention as promising candidate devices for harvesting solar energy due to flexibility, portability and low manufacturing cost [1-4]. In particular, BHJ-type PSCs developed by simply mixing electron-donating conjugated polymers and electron-accepting fullerene derivatives are the most prevalent type of PSCs due to their simple fabrication and high performance. A well-intermixed blend of the electron donor-acceptor, with small-scale separation that is comparable to the exciton diffusion length, is required in BHJ-type PSCs to ensure their high performance in the PSCs. This is because photogenerated excitons can be dissociated only at the interface between the donor and the acceptor [5,6]. However, the control of phase separation between the donor and the acceptor in the BHJ blend is not trivial because the kinetically trapped BHJ morphology is concurrently dependent on various parameters, including the intrinsic properties of the materials and the device processing conditions.

Phase separation between the donor and the acceptor is determined by both thermodynamic and kinetic parameters, such as the interfacial tension between the donor and the acceptor, the solubilities of the donor and the acceptor, and the evaporation rate of the solvent [7-11]. Hence, much research has focused on tuning the chemical structures of conjugated polymers to control the interaction between the electron-donating polymers and the electron-accepting fullerene derivatives [12-18]. Even small changes in alkyl solubilizing groups of conjugated polymers can induce significant effects on the blend morphology and the performance of the solar cell [19-23]. The importance of the structural effects of the fullerene derivatives on the BHJ blend morphology can be amplified because they have much higher molecular mobility than polymers, resulting in the tendency to diffuse out of the polymer and thus, seriously affecting the BHJ blend morphology [24-27]. Initially, the solubilizing groups of the fullerenes were modified with the aim of tuning the LUMO levels, because the open-circuit voltage (V_{oc}) of the PSCs is proportional to the difference between the lowest unoccupied molecular orbital (LUMO) level of fullerene derivatives and the highest occupied molecular orbital (HOMO) level of the electron-donating polymers [28-32]. For example, several fullerene bis-adduct derivatives have been developed recently in order to effectively increase V_{oc} and produce higher efficiencies in the PSCs [28,29,33-35], because the fullerene bis-adducts have higher LUMO energy levels than fullerene mono-adducts. The higher energy levels are due to the presence of fewer unsaturated bonds in the bis-adducts, which reduces the molecule's electron affinity. In addition, the solubilizing groups of the fullerene derivatives have been modified to improve their solubility in organic solvents and increase their miscibility with polymer donors [36-38]. For example, Troshin et al. reported the modification of ester groups in phenyl-C_{61}-butyric acid methyl ester (PCBM) because the side chains appended to the ester groups enhanced their solubility in organic solvents [39]. However, the successful modification of fullerenes resulting

†To whom correspondence should be addressed.
E-mail: bumjoonkim@kaist.ac.kr
‡This article is dedicated to Prof. Hwayong Kim on the occasion of his retirement from Seoul National Univerisity.

in improved power conversion efficiencies (PCEs) of the PSCs compared to PCBM rarely has been reported due to the changes in other properties that are accompanied by the modifications, such as changes in the electrical properties, electro-chemical properties, and crystalline behavior [31,32,40,41]. Furthermore, the effects of chemical modification of fullerene derivatives have been rarely addressed in terms of the morphological interactions with conjugated polymers, although the changes of the solubility of the fullerene derivatives could significantly affect the interfacial interactions with polymers and the blend morphology. Therefore, systematic study of the effects of the molecular structure of fullerene derivatives on their interaction with conjugated polymers and of their effects on the performances of PSCs is essential to determine the appropriate design of fullerene derivatives for use in PSCs. Such study on the molecular structure-device function relationship in PSCs using the indene-C_{60} bis-adducts (ICBA) model is especially important, because ICBA is one of the most studied and successful bis-adduct fullerenes, which produces high V_{oc} and PCE values in PSCs [33, 35,42].

Herein, we introduce three different substituents into the end solubilizing groups of ICBA molecules to produce a series of the ICBA based fullerene derivatives and study the effect of the structural changes on the blend morphology with the poly(3-hexylthiophene) (P3HT) donor polymers. The fullerene derivatives based on ICBA were chosen as a model system due to their high PCE and the simplicity in their synthetic routes [43]. Modification of the solubilizing group in ICBA was achieved by simply varying the chemical structure of the indene precursors with different end-groups: fluorine, methoxy, and bromine functional groups (Fig. 1). The introduction of these functional end-groups induced changes in the interactions with P3HT, and thus, the PCE values of P3HT : ICBA-derivative devices varied dramatically from 2.9 to 5.2%. The change in the interactions between P3HT and ICBA derivatives also was demonstrated by measuring the surface tensions of P3HT and the different ICBA derivatives and comparing the corresponding interfacial tensions between P3HT and each different ICBA derivative. In particular, the blend morphologies of P3HT and the ICBA-derivatives were dependent largely on the surface tension values of the ICBA derivatives, resulting in the significant changes in the values of fill factor (FF) and short circuit current (J_{sc}) and, thus, in the PCE values of the photovoltaic devices. In addition, the effects of the end-functional groups of the ICBA derivatives on charge transport were investigated by measuring the performance of each of the ICBA derivatives in organic field-effect transistors (OFETs).

EXPERIMENTAL

1. Materials

All commercially available reagents were used without further purification unless otherwise indicated. The organic solvents (1,2-dichlorobenzene, toluene, hexane, and methanol) were used as anhydrous solvents. Column chromatography was carried out on Merck silica gel 60 (230-400 mesh).

2. General Procedure for Synthesis of Indene Bis-adducts Fullerene Derivatives

The compounds were prepared by using a modification of a published procedure [43]. Thirty-five milliliters of indene-based precursors in 1,2-dichlorobenzene was added to a solution of C_{60}, and the mixture was stirred at reflux temperature for 2 h under an Ar atmosphere. Upon cooling to room temperature, the reaction mixture was precipitated with excess methanol. The precipitated solid was filtered and purified by flash column chromatography on silica gel using toluene/hexane as the gradient eluent to afford the corresponding fullerene derivatives.

ICBA was prepared by the reaction of C_{60} (500 mg, 0.695 mmol) with indene (970 mg, 8.34 mmol). A brown solid (272 mg, 41%) of the desired product was obtained by purification using column chromatography (hexane/toluene): Elemental analysis for $C_{78}H_{16}$: calculated: C, 98.3; H, 1.7. found: C, 97.1; H, 1.7. Matrix-assisted laser desorption/ionization–time of flight mass spectrometry (MALDI-TOF MS): calculated for $C_{78}H_{16}$ 952.962. found: 953.069 (M^+).

5-Fluoro-indene C_{60} bis-adduct (FICBA) was prepared by the reaction of C_{60} (890 mg, 1.236 mmol) with 5-fluoro-indene (1.99 g, 14.83 mmol). A brown solid (367 mg, 30%) of the desired product was obtained by purification using column chromatography (hexane/toluene): MALDI-TOF MS: calculated for $C_{78}H_{16}$ 988.943. found: 989.263 (M^+).

5-Methoxy-indene C_{60} bis-adduct (MICBA) was prepared by the reaction of C_{60} (505 mg, 0.701 mmol) with 5-methoxy-indene (1.23 g, 8.41 mmol). A brown solid (201 mg, 29%) of the desired product was obtained by purification using column chromatography (hexane/toluene): MALDI-TOF MS: calculated for $C_{80}H_{20}O_2$ 1013.014. found: 1013.955 (M^+).

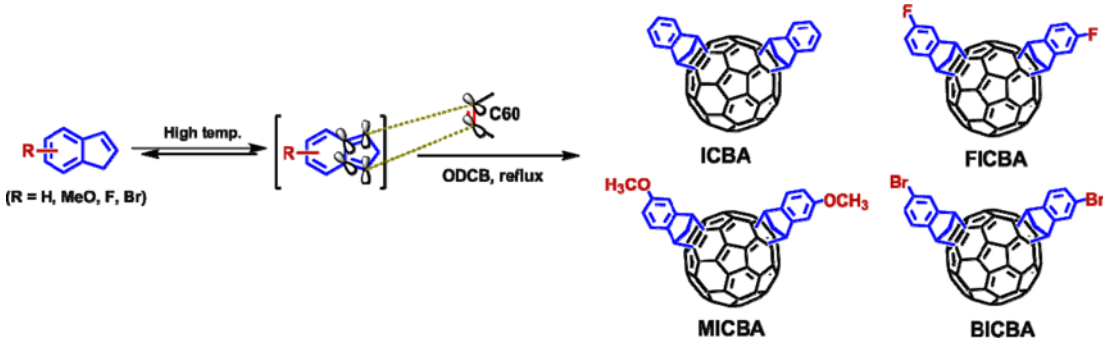

Fig. 1. Synthesis route and molecular structure of ICBA and three different ICBA derivatives.

5-Bromo-indene C_{60} bis-adduct (BICBA) was prepared by the reaction of C_{60} (700 mg, 0.972 mmol) with 5-bromo-indene (2.28 g, 11.66 mmol). A brown solid (292 mg, 27%) of the desired product was obtained by purification using column chromatography (hexane/toluene): MALDI-TOF MS: calculated for $C_{78}H_{14}Br_2$ 1110.754. found: 1110.872 (M^+).

3. PSC Fabrication

P3HT (BASF P200) was used as the electron donor, and ICBA, FICBA, MICBA, and BICBA were used as electron acceptors. Solutions of P3HT, ICBA, FICBA, MICBA, and BICBA in *o*-dichlorobenzene (30 mg mL^{-1}) were prepared and stirred at 100 °C for more than 24 h. Then, the solutions were filtered with a 0.2-μm PTFE syringe filter. Next, the P3HT solution was mixed with the solutions of the ICBA, FICBA, MICBA, and BICBA at optimized donor : acceptor ratios. The concentration of P3HT in the blend solution was 15 mg mL^{-1}. The devices were fabricated using an ITO/PEDOT : PSS/P3HT : ICBA derivatives/LiF/Al structure. ITO-coated glass substrates were ultrasonicated in acetone and 2% Helmanex soap in water, followed by ultrasonication in deionized water and then in isopropyl alcohol. Each ultrasonication step was conducted for more than 20 min. Then, the substrates were dried for several hours in an oven at 80 °C. The ITO substrates were treated with UV-ozone and a filtered dispersion of PEDOT : PSS in water (Baytron PH 500) was spin-coated at 2,000 rpm for 30 s onto the substrates and baked for 20 min at 140 °C in air. Then, all subsequent procedures were performed in a glove box under an N_2 atmosphere. Each blending solution of P3HT and fullerene derivative was spin-coated onto an ITO/PEDOT : PSS substrate at 900 rpm for 40 s. Each P3HT/fullerene derivative film was dried and the final thickness of the films was ~120 nm. Then, the substrates were placed in an evaporation chamber at high vacuum (less than 10^{-6} Torr) for more than 1 hr before evaporating approximately 0.7 nm of LiF and 100 nm of Al. The configuration of the shadow mask produced four independent devices on each substrate. All of the samples were thermally annealed at 150 °C for 5 min to optimize their device performance. The active area of each of the fabricated devices was 0.102 cm^2. The photovoltaic performance of each of the devices was characterized by using a solar simulator (ABET Technologies) with an air mass (AM) 1.5 G filter. The intensity of the solar simulator was carefully calibrated with an AIST-certified silicon photodiode, and the current-voltage behavior was measured with a Keithley 2400 SMU.

4. Fabrication of the OFETs

In a typical solution-shearing process, the fullerene films were spin-coated onto *n*-octadecyltrimethoxysilane (OTS)-treated SiO_2/Si substrates using chlorobenzene solutions (3 mg mL^{-1}) of the fullerene derivatives. An upper substrate dragged the solution placed on a heated substrate at a shearing rate of 0.12 mm s^{-1}, which was controlled by a digital syringe pump. Then, all the semiconductor films were placed in a vacuum oven at 80 °C for the complete drying. After drying, 40 nm-thick gold electrodes were thermally evaporated through a shadow mask onto the semiconductor layer. The current-voltage (I-V) characteristics of the devices were measured in a N_2-filled glovebox by using a Keithley 4200 semiconductor parametric analyzer, and their corresponding field-effect mobility was calculated in the saturation regime by the following equation:

$$I_D = \frac{W}{2L}\mu_e C_i (V_G - V_T)^2$$

where I_D is the drain current, W and L are the channel width and length of semiconductor film, respectively, μ_e is the electron mobility, C_i is the capacitance per unit area of the gate dielectric, and V_G and V_T are the gate voltage and threshold voltage, respectively.

5. Contact Angle Measurement

Static contact angles for water and glycerol were measured with a contact angle analyzer (Phoenix 150, SEO, Inc.) equipped with a microsyringe that can dispense liquid droplet. A 5 μL of liquid drop was delivered to the surface of the sample. At least 10 measurements were taken for each liquid drop to report their average values.

6. Photoluminescence (PL) Spectra Measurement

Glass substrates were ultrasonicated in acetone, followed by ultrasonication in deionized water and then in isopropyl alcohol. Each ultrasonication step was conducted for more than 20 min. Then, the substrates were dried for several hours in the oven at 80 °C. Each blend of P3HT and fullerene derivative was spin-coated onto the glass substrate at 900 rpm for 40 s. Since the concentration of P3HT in the blend solution was 15 mg mL^{-1}, diluted P3HT solution (15 mg mL^{-1}) was solely spin-coated onto the glass substrate at 900 rpm for 40 s as a control sample for PL quenching study. For each film, PL spectra were taken with a Horiba Jovin Yvon NanoLog spectrophotometer under 460 nm excitation wavelength. The PL quenching efficiency of each P3HT : ICBA-derivative film was determined by comparing its PL intensity to the PL intensity of the pristine P3HT film.

RESULTS AND DISCUSSION

The synthesis route and molecular structure of ICBA and three different ICBA derivatives are shown in Fig. 1. The various indene derivatives (indene, 5-fluoro-indene, 5-methoxy-indene, and 5-bromo-indene) were reacted with C_{60} using a modified Diels-Alder [4+2] cyclo-addition [43]. After purification with flash silica column chromatography (toluene/hexane as the gradient eluent), four different fullerene derivatives of indene C_{60} bis-adduct (ICBA), 5-fluoro-indene C_{60} bis-adduct (FICBA), 5-methoxy-indene C_{60} bis-adduct (MICBA), and 5-bromo-indene C_{60} bis-adduct (BICBA) were successfully synthesized and confirmed by MALDI-TOF mass spectroscopy and elemental analysis. For convenience, the four different ICBA derivatives are denoted as ICBA, FICBA, MICBA, and BICBA, as shown in Fig. 1.

The LUMO levels of fullerene derivatives are one of the most important factors in evaluating their potential as electron acceptors in photovoltaic cells [31,44]. The electrochemical properties of ICBA, FICBA, MICBA, and BICBA were therefore estimated using cyclic voltammetry (CV). The CV curves were measured with an Ag quasi-reference electrode and calibrated using a ferrocene/ferrocenium (Fc/Fc^+) redox couple as an external standard [12,45]. Fig. 2 shows that all of the ICBA derivatives had two distinct, quasi-reversible reduction waves in the negative potential range between –0.9 and –2.3 V; Table 1 summarizes the first (E_1) and second (E_2) reduction potentials of each fullerene derivative. The onset reduction potentials (E_{red}^{on}) and corresponding LUMO energy levels of

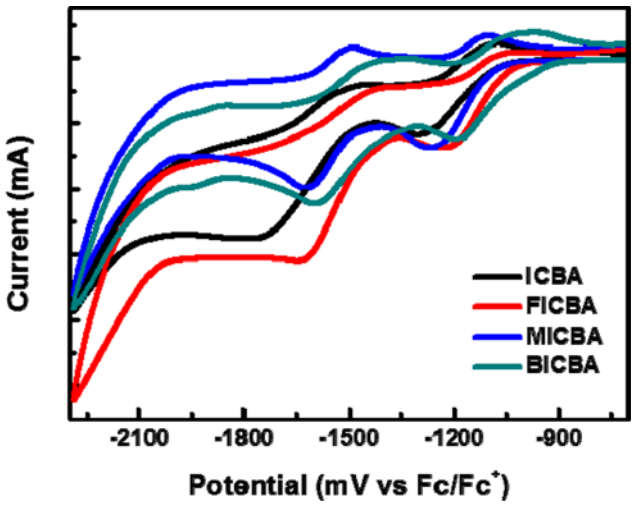

Fig. 2. Cyclic voltammetry curves for ICBA, FICBA, MICBA, and BICBA with an Ag quasi-reference electrode.

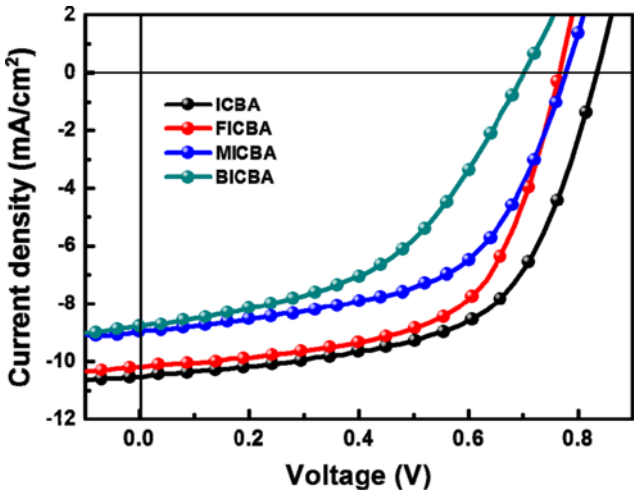

Fig. 3. Current density-voltage characteristics of P3HT : ICBA (1 : 0.6)-, P3HT : FICBA (1 : 0.7)-, P3HT : MICBA (1 : 0.8)-, and P3HT : BICBA (1 : 0.8)-based BHJ devices under AM 1.5 illumination at 100 mW cm^{-2}.

Table 1. Electrochemical properties of ICBA, FICBA, MICBA, and BICBA

Compounds	E_1 (V)	E_2 (V)	E_{red}^{on} (V)	LUMO (eV)
ICBA	−1.30	−1.74	−1.09	−3.71
FICBA	−1.24	−1.65	−1.05	−3.75
MICBA	−1.27	−1.62	−1.11	−3.69
BICBA	−1.19	−1.60	−1.00	−3.80

the fullerene derivatives are also summarized. The E_1 and E_2 of ICBA were −1.30 and −1.74 V, respectively, and the calculated LUMO level was −3.71 eV, which is comparable to those of the previous findings [29]. FICBA and BICBA exhibited greater values of E_1, E_2 and E_{red}^{on} than ICBA, resulting in the lower LUMO levels of −3.75 and −3.80 eV, respectively. However, the MICBA had slightly decreased E_{red}^{on} and, thus, a higher LUMO level (−3.69 eV) than ICBA. Hummelen et al. previously reported that the LUMO levels of PCBM derivatives were determined by the electrochemical properties of the substituents; thus, LUMO levels can be increased or decreased by the electron-donating and electron-withdrawing substituents, respectively [46]. In the same way, the methoxy group was introduced as the electron-donating substituent into the ICBA, and the LUMO level of MICBA was slightly greater than that of the ICBA, i.e., −3.69 eV compared to from −3.71 eV. In contrast, the LUMO levels of FICBA and BICBA decreased to −3.75 and −3.80 eV, respectively, due to the electro-withdrawing substituents. Therefore, the electrochemical properties of ICBA derivatives were controlled systematically by simply introducing three different functional groups into the chemical backbone of ICBA.

To investigate the relationship between the solubilizing groups in the ICBA derivatives and the performance of the PSCs, BHJ-type PSCs (ITO/PEDOT : PSS/P3HT : ICBA-derivatives/LiF/Al) were fabricated with blends of four different ICBA derivatives and electron donor, P3HT, and their performances were measured. Fig. 3 shows the current density versus voltage curves of the optimized solar cell devices under AM 1.5 illumination with intensity of 100 mW cm^{-2}. The characteristics of the PSC devices with various ratios of P3HT to each fullerene derivative are summarized in Table 2. The P3HT : ICBA device exhibited a PCE of 5.21% (V_{oc} of 0.83 V, J_{sc} of 10.53 mA cm^{-2}, and FF of 0.59), which was in good agreement with that of previous report [29]. However, the PCE values of P3HT : ICBA-derivative devices varied widely from 2.85 to 4.64% and, thus, the optimized PCE values increased in the order of BICBA (PCE=2.94%), MICBA (PCE=3.92%) and FICBA (PCE=4.64%). Compared to the P3HT : ICBA devices, the V_{oc} values of the optimized P3HT : FICBA and P3HT : BICBA devices decreased to 0.77 and 0.70 V, respectively, due to the lower-lying LUMO levels of FICBA and BICBA.

Table 2. Characteristics of PSC devices composed of P3HT : ICBA, P3HT : FICBA, P3HT : MICBA, and P3HT : BICBA under AM 1.5 G-simulated solar illumination (100 mW cm^{-2})

Active layer (w/w)	V_{oc} (V)	J_{sc} (mA/cm^2)	FF	PCE (%)
P3HT : ICBA (1 : 0.6)	0.83	10.53	0.59	5.21
P3HT : FICBA (1 : 0.6)	0.76	9.89	0.60	4.54
P3HT : FICBA (1 : 0.7)	0.77	9.98	0.61	4.64
P3HT : MICBA (1 : 0.7)	0.81	8.94	0.53	3.80
P3HT : MICBA (1 : 0.8)	0.78	8.96	0.56	3.92
P3HT : BICBA (1 : 0.7)	0.73	8.65	0.45	2.85
P3HT : BICBA (1 : 0.8)	0.70	8.78	0.48	2.94

To better understand the changes in the performance of the PSCs made of different ICBA-derivatives, the surface tensions of P3HT and fullerene derivatives were calculated by contact angle measurements. The contact angles of two different solvents, water and glycerol, on the P3HT and ICBA-derivatives films were measured. The surface tension of each film was calculated using the Wu model and the following equations [47,48]:

$$\gamma_{water}(1+\cos\theta_{water}) = \frac{4\gamma_{water}^{d}\gamma^{d}}{\gamma_{water}^{d}+\gamma^{d}} + \frac{4\gamma_{water}^{p}\gamma^{p}}{\gamma_{water}^{p}+\gamma^{p}} \quad (1)$$

Table 3. Contact angles of water and glycerol on P3HT and ICBA-derivatives films; surface tension values of P3HT and ICBA derivatives films; interfacial tensions between P3HT and each different ICBA derivative

Compounds	θ_{water} (deg)	$\theta_{glycerol}$ (deg)	Surface tension (mN m^{-1})	γ (mN m^{-1})[a]
P3HT	97.1	93.2	20.5	-
ICBA	93.8	79.7	27.1	6.4
FICBA	89.7	76.7	28.3	4.9
MICBA	89.2	73.8	30.4	7.3
BICBA	88.6	71.1	32.6	8.3

[a]Interfacial tension between P3HT and each fullerene derivative

$$\gamma_{glycerol}(1+\cos\theta_{glycerol}) = \frac{4\gamma^{d}_{glycerol}\gamma^{d}}{\gamma^{d}_{glycerol}+\gamma^{d}} + \frac{4\gamma^{p}_{glycerol}\gamma^{p}}{\gamma^{p}_{glycerol}+\gamma^{p}} \quad (2)$$

$$\gamma^{total} = \gamma^{d} + \gamma^{p} \quad (3)$$

where γ^{total} is the total surface tension of P3HT and the ICBA derivatives; γ^{d} and γ^{p} are the dispersion and polar components of γ^{total}, respectively; γ_i is the total surface tension of the i material (i=water or glycerol); γ_i^{d} and γ_i^{p} are the dispersion and polar components of γ_i, respectively, and θ is the contact angle of the droplet (water or glycerol) on the P3HT and ICBA-derivatives films.

The measured contact angles of water and glycerol on each film and the corresponding surface tensions were summarized in Table 3. The contact angle of a pristine P3HT film was measured as control sample and the film had a surface tension of 20.5 mN m^{-1}, which was calculated based on θ_{water}=97.1° and $\theta_{glycerol}$=93.2°. The measured surface tension value of P3HT was well matched with that of the literature value [38,49,50]. The ICBA derivatives exhibited decreasing trend of water contact angles in the order of ICBA (93.8°), FICBA (89.7°), MICBA (89.2°), and BICBA (88.6°), and the contact angles of glycerol showed a similar trend in the same order. As a result, the surface tension of ICBA derivatives decreased in the order of BICBA, MICBA, FICBA, and ICBA, ranging from 32.6 to 27.1 mN m^{-1}. Since the surface tension of P3HT film was much lower than that of each ICBA derivative, it was anticipated that the P3HT would be abundant on the top of the P3HT : ICBA-derivative layer to minimize the surface energy of the blend film, leading to a P3HT-rich phase on the top and a ICBA derivative-rich phase at the bottom of active layer [51]. Also, the larger difference in the surface tension between P3HT and ICBA derivatives in P3HT : MICBA and P3HT : BICBA devices can induce severe phase separation in the blend film.

In the BHJ-type blend system of electron donor and acceptor, the interfacial tension (γ) between two materials determines their miscibility [52]. To elucidate the relationship between the miscibility and the performances of the PSCs, the interfacial tension between P3HT and each ICBA derivative was calculated by using the following equation [48]:

$$\gamma_{12} = \gamma_1 + \gamma_2 - \frac{4\gamma_1^{d}\gamma_2^{d}}{\gamma_1^{d}+\gamma_2^{d}} - \frac{4\gamma_1^{p}\gamma_2^{p}}{\gamma_1^{p}+\gamma_2^{p}} \quad (4)$$

where γ_{12} is the interfacial tension between P3HT (1) and each ICBA derivative (2); γ_j is the surface tension of the j material (j=1 or 2), and the dispersion and polar components of γ_j are denoted as γ_j^{d} and γ_j^{p} that are calculated using the contact angle of water and glycerol droplet on the P3HT and ICBA derivatives films.

The calculated interfacial tensions between the P3HT and the four different ICBA derivatives are summarized in Table 3. As the surface tensions of the ICBA derivatives varied, the interfacial tensions were significantly changed. The interfacial tension between P3HT and FICBA showed the smallest γ value of 4.9 mN m^{-1}. In contrast, the MICBA and BICBA with P3HT (γ=7.3 and 8.3 mN m^{-1}, respectively) showed much higher interfacial tension than that of the P3HT : ICBA blend system. In general, the blend system with low γ value between two materials can develop a well-mixed interpenetrating network with much smaller energy penalty than the blend with high γ value. Thus, the P3HT : ICBA and P3HT : FICBA blend exhibited higher FF (0.59 and 0.61 for P3HT : ICBA device and P3HT : FICBA device, respectively) and J_{sc} values due to their well-developed interpenetrating network with large interfacial area. From the same perspective, the P3HT : MICBA and P3HT : BICBA blend systems having high γ values would have smaller interfacial area and suppress the exciton dissociation at the interface, which resulted in the significant decreases in FF, J_{sc} and the corresponding PCEs. Thus, the morphological differences caused by the changes in the interfacial tension within each P3HT : ICBA-derivative film can affect charge separation and charge transfer ability between P3HT and ICBA derivatives.

Steady-state PL measurements were performed to gain evidence of changes in the charge transfer from P3HT to the ICBA derivatives and the blend morphology with regard to the interfacial tension. Fig. 4 shows the room temperature PL spectra of P3HT, P3HT : ICBA, P3HT : FICBA, P3HT : MICBA, and P3HT : BICBA films, obtained with an excitation wavelength of 460 nm. The P3HT : ICBA-derivative blend samples were prepared by spin-coating the blend solution on glass substrates with the optimized conditions applied to the fabrication of solar cell devices. The PL quenching efficiency of each P3HT : ICBA-derivative film was calculated by comparing its PL intensity with that of the pristine P3HT film. When the P3HT

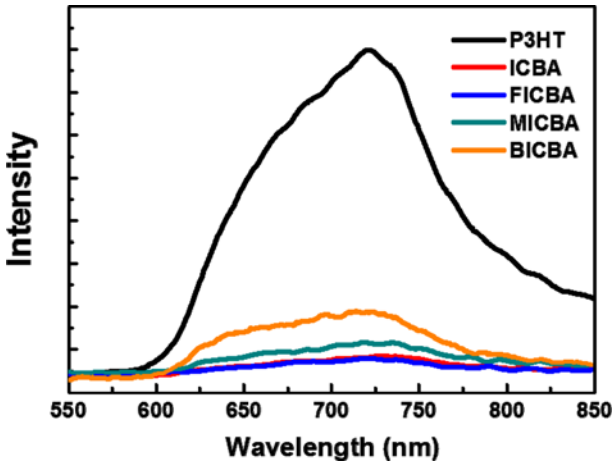

Fig. 4. Static photoluminescence spectra (excitation wavelength of 460 nm) of P3HT, P3HT : ICBA, P3HT : FICBA, P3HT : MICBA, and P3HT : BICBA films.

Table 4. Electrical performance of OFET devices based on the solution-sheared thin films of ICBA derivatives[a]

Compounds	$\mu_{e,max}$ ($cm^2\ V^{-1}\ s^{-1}$)[b]	$\mu_{e,avg}$ ($cm^2\ V^{-1}\ s^{-1}$)[c]	I_{on}/I_{off}	V_T (V)
ICBA	3.50×10^{-3}	3.40×10^{-3}	7.5×10^{4}	30.7
FICBA	1.03×10^{-3}	9.97×10^{-4}	2.4×10^{5}	21.8
MICBA	1.47×10^{-4}	1.37×10^{-4}	2.7×10^{3}	8.1
BICBA	8.12×10^{-5}	6.97×10^{-5}	5.9×10^{3}	20.3

[a]I-V characteristics were measured in N_2-filled glovebox
[b]Maximum mobility of the OFET devices
[c]Average mobility of the OFET devices

was blended with the ICBA derivatives, the PL spectra were dramatically changed compared to the PL spectrum of the pristine P3HT. In particular, the emissions of the P3HT : ICBA and P3HT : FICBA films were quenched by 90% and 89%, respectively, relative to the pristine P3HT. However, the quenching ratios of the emissions of P3HT : MICBA and P3HT : BICBA were reduced to 86% and 78%, respectively. These decreased PL quenching abilities suggested that poor charge transfer occurred through the interface in the P3HT : MICBA and P3HT : BICBA films [20,53-55]. In addition, the decreasing trend of PL quenching efficiency between P3HT and ICBA derivatives was in accordance with the trend in γ values, because the morphology of the blend film with smaller interfacial tension created greater interfacial area, which allowed for efficient charge transfer between the donor and acceptor domains.

The field-effect mobility of each ICBA derivative was investigated to better understand the effect of the structural changes of the ICBA derivatives on their charge transport. The OFETs were fabricated with top-contact, bottom-gate geometry. The I-V characteristics of the OFETs of the ICBA derivatives are summarized in Table 4. The ICBA devices exhibited an average electron mobility of $3.40\times10^{-3}\ cm^2\ V^{-1}\ s^{-1}$, which agreed well with the previous findings [42]. The average electron mobility of FICBA devices was $9.97\times10^{-4}\ cm^2\ V^{-1}\ s^{-1}$, and the maximum electron mobility ($\mu_{e,max}$= $1.03\times10^{-3}\ cm^2\ V^{-1}\ s^{-1}$) was comparable to that of the ICBA devices. However, the MICBA and BICBA devices showed serious decreases in both the average and the maximum electron mobility. Specifically, the maximum electron mobility of the MICBA devices decreased by an order of magnitude compared to those of the ICBA and FICBA derivatives, and the maximum electron mobility of the BICBA devices decreased by two orders of magnitude. The reduced electron mobility of the MICBA and BICBA devices could induce poor charge transport through the fullerene domains in the blend film of the PSCs, which could be one of the reasons for the decreased current density of P3HT : MICBA and P3HT : BICBA solar cell devices. Also, it was concluded that even slight modification of the solubilizing group of the fullerene derivatives can affect their charge transport properties, which might be attributed to the changes in their molecular packing structures [56-58].

CONCLUSIONS

We successfully synthesized a series of ICBA-based fullerene derivatives with different functional end-groups: fluorine, methoxy and bromine groups. By simply varying the end-groups of the ICBA derivatives, the electrochemical and physical properties of the ICBA derivatives were systematically tuned. In particular, the miscibility and interfacial tension of the ICBA derivatives with P3HT were easily controlled due to the change in the surface tension of each ICBA derivative. Therefore, as the interfacial tension between P3HT and each of the ICBA derivative was reduced, the FF and J_{sc} values of the P3HT : ICBA-derivative devices increased gradually, which resulted in changes in the PCE ranging from 2.9 to 5.2%. The change in the charge transport of the P3HT : ICBA-derivative devices due to the modification of the functional end-groups was supported by comparing the electron mobility of each of the ICBA derivative in the OFETs. Our findings provide a model system for understanding the relationship between the structure of electron acceptors and the PSC performance.

ACKNOWLEDGEMENTS

This research was supported by the New & Renewable Energy Program of KETEP Grant (20133030000130, 20133030011330), funded by the Ministry of Trade, industry & Energy, Republic of Korea. This research was also supported by the National Research Foundation Grant (2012M1A2A2671746), funded by the Korean Government. Authors also acknowledge the KAIST-KUSTAR Research Project and Samsung Display Co. for the financial support.

REFERENCES

1. F. C. Krebs, S. A. Gevorgyan and J. Alstrup, *J. Mater. Chem.*, **19**, 5442 (2009).
2. A. C. Arias, J. D. MacKenzie, I. McCulloch, J. Rivnay and A. Salleo, *Chem. Rev.*, **110**, 3 (2010).
3. B. C. Thompson and J. M. J. Fréchet, *Angew. Chem., Int. Ed.*, **47**, 58 (2008).
4. J. A. Hauch, P. Schilinsky, S. A. Choulis, R. Childers, M. Biele and C. J. Brabec, *Sol. Energy Mater. Sol. Cells*, **92**, 727 (2008).
5. W. Ma, C. Yang, X. Gong, K. Lee and A. J. Heeger, *Adv. Funct. Mater.*, **15**, 1617 (2005).
6. D. R. Kozub, K. Vakhshouri, L. M. Orme, C. Wang, A. Hexemer and E. D. Gomez, *Macromolecules*, **44**, 5722 (2011).
7. G. Li, Y. Yao, H. Yang, V. Shrotriya, G. Yang and Y. Yang, *Adv. Funct. Mater.*, **17**, 1636 (2007).
8. Y. Yao, J. Hou, Z. Xu, G. Li and Y. Yang, *Adv. Funct. Mater.*, **18**, 1783 (2008).
9. J. Peet, M. L. Senatore, A. J. Heeger and G. C. Bazan, *Adv. Mater.*, **21**, 1521 (2009).
10. J. K. Lee, W. L. Ma, C. J. Brabec, J. Yuen, J. S. Moon, J. Y. Kim, K. Lee, G. C. Bazan and A. J. Heeger, *J. Am. Chem. Soc.*, **130**, 3619 (2008).
11. S. J. Lou, J. M. Szarko, T. Xu, L. Yu, T. J. Marks and L. X. Chen, *J. Am. Chem. Soc.*, **133**, 20661 (2011).
12. C.-H. Cho, H. Kang, T. E. Kang, H.-H. Cho, S. C. Yoon, M.-K. Jeon and B. J. Kim, *Chem. Commun.*, **47**, 3577 (2011).
13. S. Ko, E. Verploegen, S. Hong, R. Mondal, E. T. Hoke, M. F. Toney, M. D. McGehee and Z. Bao, *J. Am. Chem. Soc.*, **133**, 16722 (2011).
14. Y.-J. Cheng, C.-H. Chen, Y.-S. Lin, C.-Y. Chang and C.-S. Hsu,

Chem. Mater., **23**, 5068 (2011).
15. H. J. Son, W. Wang, T. Xu, Y. Liang, Y. Wu, G. Li and L. Yu, *J. Am. Chem. Soc.*, **133**, 1885 (2011).
16. I. Osaka, M. Shimawaki, H. Mori, I. Doi, E. Miyazaki, T. Koganezawa and K. Takimiya, *J. Am. Chem. Soc.*, **134**, 3498 (2012).
17. T. E. Kang, H.-H. Cho, H. J. Kim, W. Lee, H. Kang and B. J. Kim, *Macromolecules*, **46**, 6806 (2013).
18. H.-H. Cho, T. E. Kang, K.-H. Kim, H. Kang, H. J. Kim and B. J. Kim, *Macromolecules*, **45**, 6415 (2012).
19. J. M. Szarko, J. Guo, Y. Liang, B. Lee, B. S. Rolczynski, J. Strzalka, T. Xu, S. Loser, T. J. Marks, L. Yu and L. X. Chen, *Adv. Mater.*, **22**, 5468 (2010).
20. J. S. Kim, Y. Lee, J. H. Lee, J. H. Park, J. K. Kim and K. Cho, *Adv. Mater.*, **22**, 1355 (2010).
21. J. K. Park, J. Jo, J. H. Seo, J. S. Moon, Y. D. Park, K. Lee, A. J. Heeger and G. C. Bazan, *Adv. Mater.*, **23**, 2430 (2011).
22. C.-H. Cho, H. J. Kim, H. Kang, T. J. Shin and B. J. Kim, *J. Mater. Chem.*, **22**, 14236 (2012).
23. C. Piliego, T. W. Holcombe, J. D. Douglas, C. H. Woo, P. M. Beaujuge and J. M. J. Fréchet, *J. Am. Chem. Soc.*, **132**, 7595 (2010).
24. H. J. Kim, A. R. Han, C.-H. Cho, H. Kang, H.-H. Cho, M. Y. Lee, J. M. J. Fréchet, J. H. Oh and B. J. Kim, *Chem. Mater.*, **24**, 215 (2011).
25. Y.-J. Cheng, C.-H. Hsieh, P.-J. Li and C.-S. Hsu, *Adv. Funct. Mater.*, **21**, 1723 (2011).
26. X. Yang, J. K. J. van Duren, R. A. J. Janssen, M. A. J. Michels and J. Loos, *Macromolecules*, **37**, 2151 (2004).
27. A. Swinnen, I. Haeldermans, M. vandeVen, J. D'Haen, G. Vanhoyland, S. Aresu, M. D'Olieslaeger and J. Manca, *Adv. Funct. Mater.*, **16**, 760 (2006).
28. K.-H. Kim, H. Kang, S. Y. Nam, J. Jung, P. S. Kim, C.-H. Cho, C. Lee, S. C. Yoon and B. J. Kim, *Chem. Mater.*, **23**, 5090 (2011).
29. H. Kang, C.-H. Cho, H.-H. Cho, T. E. Kang, H. J. Kim, K.-H. Kim, S. C. Yoon and B. J. Kim, *ACS Appl. Mater. Interfaces*, **4**, 110 (2011).
30. C. Liu, S. Xiao, X. Shu, Y. Li, L. Xu, T. Liu, Y. Yu, L. Zhang, H. Liu and Y. Li, *ACS Appl. Mater. Interfaces*, **4**, 1065 (2012).
31. A. Varotto, N. D. Treat, J. Jo, C. G. Shuttle, N. A. Batara, F. G. Brunetti, J. H. Seo, M. L. Chabinyc, C. J. Hawker, A. J. Heeger and F. Wudl, *Angew. Chem., Int. Ed.*, **50**, 5166 (2011).
32. S. A. Backer, K. Sivula, D. F. Kavulak and J. M. J. Fréchet, *Chem. Mater.*, **19**, 2927 (2007).
33. G. Zhao, Y. He and Y. Li, *Adv. Mater.*, **22**, 4355 (2010).
34. M. Lenes, G.-J. A. H. Wetzelaer, F. B. Kooistra, S. C. Veenstra, J. C. Hummelen and P. W. M. Blom, *Adv. Mater.*, **20**, 2116 (2008).
35. Y. He, H.-Y. Chen, J. Hou and Y. Li, *J. Am. Chem. Soc.*, **132**, 1377 (2010).
36. N. D. Treat, A. Varotto, C. J. Takacs, N. Batara, M. Al-Hashimi, M. J. Heeney, A. J. Heeger, F. Wudl, C. J. Hawker and M. L. Chabinyc, *J. Am. Chem. Soc.*, **134**, 15869 (2012).
37. B. A. Collins, E. Gann, L. Guignard, X. He, C. R. McNeill and H. Ade, *J. Phys. Chem. Lett.*, **1**, 3160 (2010).
38. K.-H. Kim, H. Kang, H. J. Kim, P. S. Kim, S. C. Yoon and B. J. Kim, *Chem. Mater.*, **24**, 2373 (2012).
39. J. Y. Mayorova, S. L. Nikitenko, P. A. Troshin, S. M. Peregudova, A. S. Peregudov, M. G. Kaplunov and R. N. Lyubovskaya, *Mendeleev Commun.*, **17**, 175 (2007).
40. Y. He, C. Chen, E. Richard, L. Dou, Y. Wu, G. Li and Y. Yang, *J. Mater. Chem.*, **22**, 13391 (2012).
41. H. Zhao, X. Guo, H. Tian, C. Li, Z. Xie, Y. Geng and F. Wang, *J. Mater. Chem.*, **20**, 3092 (2010).
42. H. Kang, K.-H. Kim, T. E. Kang, C.-H. Cho, S. Park, S. C. Yoon and B. J. Kim, *ACS Appl. Mater. Interfaces*, **5**, 4401 (2013).
43. A. Puplovskis, J. Kacens and O. Neilands, *Tetrahedron Lett.*, **38**, 285 (1997).
44. C. J. Brabec, A. Cravino, D. Meissner, N. S. Sariciftci, T. Fromherz, M. T. Rispens, L. Sanchez and J. C. Hummelen, *Adv. Funct. Mater.*, **11**, 374 (2001).
45. Y.-T. Chang, S.-L. Hsu, G.-Y. Chen, M.-H. Su, T. A. Singh, E. W.-G. Diau and K.-H. Wei, *Adv. Funct. Mater.*, **18**, 2356 (2008).
46. F. B. Kooistra, J. Knol, F. Kastenberg, L. M. Popescu, W. J. H. Verhees, J. M. Kroon and J. C. Hummelen, *Org. Lett.*, **9**, 551 (2007).
47. J. Comyn, *Int. J. Adhes. Adhes*, **12**, 145 (1992).
48. S. Wu, *J. Polym. Sci., Part C: Polym. Symp.*, **34**, 19 (1971).
49. J. B. Kim, K. Allen, S. J. Oh, S. Lee, M. F. Toney, Y. S. Kim, C. R. Kagan, C. Nuckolls and Y.-L. Loo, *Chem. Mater.*, **22**, 5762 (2010).
50. J. Y. Oh, W. S. Jang, T. I. Lee, J.-M. Myoung and H. K. Baik, *Appl. Phys. Lett.*, **98**, 023303 (2011).
51. M. Campoy-Quiles, T. Ferenczi, T. Agostinelli, P. G. Etchegoin, Y. Kim, T. D. Anthopoulos, P. N. Stavrinou, D. D. C. Bradley and J. Nelson, *Nat. Mater.*, **7**, 158 (2008).
52. M. J. Rosen, *Surfactants and interfacial phenomena*, John Wiley & Sons, Inc., New York, i (2004).
53. J.-L. Wu, F.-C. Chen, Y.-S. Hsiao, F.-C. Chien, P. Chen, C.-H. Kuo, M. H. Huang and C.-S. Hsu, *ACS Nano*, **5**, 959 (2011).
54. M. M. Alam and S. A. Jenekhe, *Chem. Mater.*, **16**, 4647 (2004).
55. J. J. Dittmer, E. A. Marseglia and R. H. Friend, *Adv. Mater.*, **12**, 1270 (2000).
56. P. Wang, K. Yao, L. Chen, Y. Chen, F. Li, H. Wang and S. Yu, *Sol. Energy Mater. Sol. Cells*, **97**, 34 (2012).
57. Y. Matsuo, Y. Sato, T. Niinomi, I. Soga, H. Tanaka and E. Nakamura, *J. Am. Chem. Soc.*, **131**, 16048 (2009).
58. L. Chen, K. Yao and Y. Chen, *J. Mater. Chem.*, **22**, 18768 (2012).